J. Fluid Mech. (2012), *vol.* 696, *pp.* 263–284. © Cambridge University Press 2012
doi:10.1017/jfm.2012.34

Plume flows in porous media driven by horizontal differential heating

P. Adamou-Graham and P. G. Daniels†

Centre for Mathematical Science, City University London, Northampton Square, London EC1V 0HB, UK

(Received 21 March 2011; revised 3 January 2012; accepted 13 January 2012; first published online 6 March 2012)

In this paper we describe flow through a porous medium in a two-dimensional rectangular cavity driven by differential heating of the impermeable lower surface. The upper surface is held at constant pressure and at a constant temperature equal to the minimum temperature of the lower surface, while the sidewalls are impermeable and thermally insulated. Numerical results for general values of the Darcy–Rayleigh number R and the cavity aspect ratio A are compared with theoretical predictions for the small Darcy–Rayleigh number limit ($R \to 0$) where the temperature field is conduction-dominated, and with a boundary-layer theory for the large Darcy–Rayleigh number limit ($R \to \infty$) where convection is significant. In the latter case a horizontal boundary layer near the lower surface conveys fluid to the hot end of the cavity where it rises to the upper surface in a narrow plume. Predictions are made of the vertical heat transfer through the cavity.

Key words: convection, convection in cavities, convection in porous media

1. Introduction

One of the geophysical applications of thermal convection in porous media is to geothermal energy systems where groundwater near the Earth's surface is heated in regions of volcanic or seismic activity. Successful exploitation of such naturally occurring energy sources motivates the development of an accurate model of heat transport within the system and an understanding of the structure of the plume flows involved (see, for example, Phillips 1991).

Previous studies of thermal convection in porous media can be divided into two main groups, those where heating is from below and flow is generated typically by an instability mechanism of the type first discussed by Horton & Rogers (1945) and reviewed, for example, by Rees (2000), and those where the heating is from the side and horizontal thermal gradients generate motion. In the latter case, recent studies by Daniels & Punpocha (2004, 2005) have considered two-dimensional cavity flows with impermeable boundaries where one horizontal boundary is differentially heated and the other three boundaries are thermally insulated. For large Darcy–Rayleigh numbers R (defined in (2.4) below) the structure of such flows for a monotonic temperature distribution along the lower boundary consists of a circulation in which fluid is transported to the hot end of the lower surface within a horizontal boundary layer

† Email address for correspondence: p.g.daniels@city.ac.uk

https://doi.org/10.1017/jfm.2012.34 Published online by Cambridge University Press

of depth $R^{-1/3}$ where it is entrained into a vertical boundary layer of the same depth, rises and is then detrained back into the horizontal boundary layer. Thus, the main circulation within the cavity is confined to depths of order $R^{-1/3}$ from the heated surface, and the remainder of the cavity contains a weak circulation at a constant core temperature a little less than that of the maximum temperature of the lower surface.

The flows discussed by Daniels & Punpocha (2004, 2005) all have zero net vertical heat transfer. Flows driven from below by buoyancy forces or horizontal differential heating in which the upper surface is isothermal generally have non-zero vertical heat transfer and are more relevant to the flows that occur in geothermal energy reservoirs. The transport of heat to the upper surface requires significant flow and temperature variations across the entire height of the cavity and at high Darcy–Rayleigh numbers this generally occurs via a narrow plume. Phillips (1991, Ch. 7.6) discusses the two-dimensional plume driven by symmetrical heating from below where the ambient (upper surface) temperature is generally viewed as specified at a level below that of the heat source and there is a net upward heat flux through the system. The sidewalls are assumed impermeable and thermally insulated, and results are presented for a range of Darcy–Rayleigh numbers and aspect ratios. The similarity solution for a vertical plume in a porous medium was first given by Wooding (1963) and studies of boundary layer flows on heated vertical surfaces in porous media have been made by Merkin (1980), Ingham, Merkin & Pop (1982), Joshi & Gebhart (1984) and Ingham & Brown (1986). Related corner flows have been discussed by Daniels & Simpkins (1984), Ingham & Pop (1987) and Rees & Bassom (1991). Boundary layer flows on horizontal surfaces in porous media have been studied by Rees & Bassom (1993, 1994).

In general, if the upper surface is impermeable and held at a constant temperature less than the core temperature of the equivalent thermally insulated problem, numerical simulations (Daniels 2007) indicate that the flow develops a complex structure at large Darcy–Rayleigh numbers associated with the statically unstable vertical temperature variation across the cavity. In the present paper this statically unstable situation is explored further, but for an upper surface held at constant pressure. This is relevant to the flow in a geothermal energy reservoir where the upper surface is exposed to atmospheric pressure. This means that flow generally occurs into and out of the upper surface, where it is assumed to be transported via run-off within a shallow zone of surface water overlying the reservoir. It is also relevant to groundwater flows in submerged banks such as the Florida plateau (Kohout 1965) where the upper surface pressure and temperature are determined by the hydrostatic pressure and temperature of the surrounding seawater. A detailed discussion of the conditions applicable to such flows is given by Phillips (1991, Ch. 7). It is found that the flow adopts a boundary layer structure at high values of R and it is possible to use asymptotic methods to predict the flow and temperature fields and the heat transfer of the system. The problem is formulated in § 2 and the solution for small values of the Darcy–Rayleigh number is presented in § 3. Numerical solutions for general values of R are presented in § 4 and the asymptotic structure of the solution for large R is considered in § 5. The results are summarized and discussed in terms of their relevance to geothermal systems in § 6.

https://doi.org/10.1017/jfm.2012.34 Published online by Cambridge University Press

2. Formulation

A two-dimensional rectangular cavity $0 \leqslant x^* \leqslant d, 0 \leqslant z^* \leqslant h$ is filled with a fluid-saturated porous medium. The lower boundary $z^* = 0$ is held at temperature

$$T^* = T_0^* + \Delta T S(x^*/d), \tag{2.1}$$

where the function $S(x^*/d)$ varies monotonically from zero at $x^* = 0$ to 1 at $x^* = d$. The vertical walls $x^* = 0$ and $x^* = d$ are impermeable and thermally insulated and the upper surface $z^* = h$ is held at constant pressure and temperature T_0^*. Subject to Darcy's law and the Oberbeck–Boussinesq approximation (see, for example, Nield & Bejan 1999) steady two-dimensional motion is governed by the non-dimensional equations

$$\nabla^2 \psi = -R \frac{\partial T}{\partial x}, \tag{2.2}$$

$$\nabla^2 T = \frac{\partial (T, \psi)}{\partial (x, z)}. \tag{2.3}$$

Here $\psi = \psi(x, z)$ is the stream function non-dimensionalized by the thermal diffusivity κ, $T = T(x, z)$ is the temperature measured relative to T_0^* and non-dimensionalized by ΔT, (x, z) are Cartesian coordinates non-dimensionalized by d and R is the Darcy–Rayleigh number defined by

$$R = \frac{Kg\gamma \Delta T d}{\kappa \nu}, \tag{2.4}$$

where K is the permeability, γ is the coefficient of thermal expansion, ν is the kinematic viscosity and g is the acceleration due to gravity. The non-dimensional velocity components in the x, z directions are given by

$$u = \frac{\partial \psi}{\partial z}, \quad w = -\frac{\partial \psi}{\partial x}, \tag{2.5}$$

respectively.

The cavity sidewalls are impermeable and thermally insulated so that

$$\psi = 0, \quad \frac{\partial T}{\partial x} = 0 \quad \text{on } x = 0, 1. \tag{2.6}$$

At the impermeable lower surface

$$\psi = 0, \quad T = S(x) \quad \text{on } z = 0 \tag{2.7}$$

and at the upper surface

$$\frac{\partial \psi}{\partial z} = 0, \quad T = 0 \quad \text{on } z = A, \tag{2.8}$$

where $A = h/d$ is the aspect ratio of the cavity. Here the condition on $\partial \psi / \partial z$ represents the fact that the surface pressure is constant, given that its horizontal gradient is proportional to u, from Darcy's law.

One of the key properties of the system is the vertical heat transfer. Integration of (2.3) from $x = 0$ to $x = 1$ and use of the conditions (2.6) shows that the vertical heat flux

$$Q = -\int_0^1 \left(\frac{\partial T}{\partial z} + T \frac{\partial \psi}{\partial x} \right) \mathrm{d}x \tag{2.9}$$

https://doi.org/10.1017/jfm.2012.34 Published online by Cambridge University Press

is a constant, independent of z. The total heat transfer through the lower surface is equal to that through the upper surface because no heat escapes through the sides of the cavity. The determination of Q as a function of the two non-dimensional parameters R and A for a given temperature profile $S(x)$ is one of the main objectives of the present study. Numerical results for general values of R focus on the case of a square cavity ($A = 1$) but limiting structures for small and large values of R are found for general values of A. In terms of relevance to physical systems, the conditions (2.8) are consistent with those applicable at the upper surface of a submerged bank or geothermal reservoir subject to a constant ambient temperature T_0^*. In an experimental setting this might be achieved approximately using a porous matrix submerged at the base of a cooled water tank, with comparable Darcy–Rayleigh numbers achieved using an enhanced permeability to offset the reduction in length scale involved. An approximation to the lower surface conditions (2.7) could be achieved using an array of heating elements. In the geothermal setting the base temperature profile would be determined by the structure, shape and depth of the underlying magma chamber. Here the main assumption is that the major source of heat is positioned below (and possibly beyond) the boundary at $x^* = d$, so that the maximum temperature of the lower boundary occurs at $x^* = d, z^* = 0$. Most of the results presented here are for the quadratic profile

$$S(x) = x^2 \tag{2.10}$$

as this facilitates a simplification of the horizontal boundary layer problem at large values of R. Results have also been obtained for other profiles and are mentioned briefly below but provided the profile is monotonically increasing with x the main features of the solution are unchanged. From (2.6), the line $x^* = d$ can also be viewed as a line of symmetry with the solution for ψ and T extended as odd and even functions respectively for $x^* > d$.

3. Solution for small Darcy–Rayleigh numbers

The solution of the system (2.2), (2.3) and (2.6)–(2.8) can be expanded in the form

$$T = T_0 + RT_1 + \cdots, \quad \psi = R\psi_1 + R^2\psi_2 + \cdots \tag{3.1}$$

as $R \to 0$, where T_0 satisfies Laplace's equation

$$\frac{\partial^2 T_0}{\partial x^2} + \frac{\partial^2 T_0}{\partial z^2} = 0, \tag{3.2}$$

to be solved subject to

$$\frac{\partial T_0}{\partial x} = 0 \quad \text{on } x = 0, 1, \tag{3.3}$$

$$T_0 = S(x) \quad \text{on } z = 0, \quad T_0 = 0 \quad \text{on } z = A. \tag{3.4}$$

For the quadratic profile (2.10) the solution is readily obtained by the separation of variables as

$$T_0 = \frac{1}{3}\left(1 - \frac{z}{A}\right) + \frac{4}{\pi^2}\sum_{n=1}^{\infty} \frac{(-1)^n}{n^2}\{\cosh(n\pi z) - \coth(n\pi A)\sinh(n\pi z)\}\cos(n\pi x). \tag{3.5}$$

https://doi.org/10.1017/jfm.2012.34 Published online by Cambridge University Press

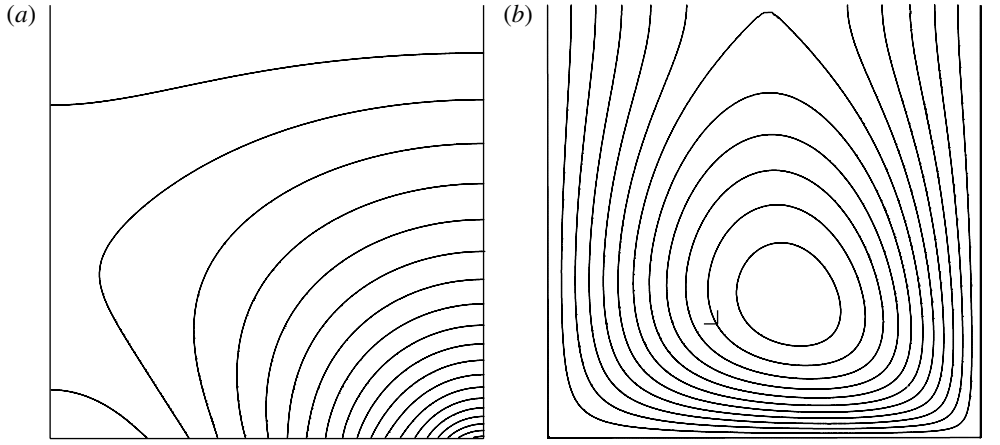


FIGURE 1. Contours of T_0 (*a*) and ψ_1 (*b*) for a square cavity ($A = 1$) with the quadratic temperature profile (2.10).

This conductive temperature field generates motion via the equation

$$\frac{\partial^2 \psi_1}{\partial x^2} + \frac{\partial^2 \psi_1}{\partial z^2} = -\frac{\partial T_0}{\partial x}, \tag{3.6}$$

to be solved subject to

$$\psi_1 = 0 \quad \text{on } x = 0, 1, \tag{3.7}$$

$$\psi_1 = 0 \quad \text{on } z = 0, \qquad \frac{\partial \psi_1}{\partial z} = 0 \quad \text{on } z = A. \tag{3.8}$$

The required solution is

$$\psi_1 = \frac{2}{\pi^2} \sum_{n=1}^{\infty} \frac{(-1)^n}{n^2} \left(z(\sinh(n\pi z) - \coth(n\pi A)\cosh(n\pi z)) + \frac{2\sinh(n\pi z)}{n\pi \sinh(2n\pi A)} \right) \sin(n\pi x). \tag{3.9}$$

Contours of T_0 and ψ_1 are shown in figure 1 for the case of a square cavity ($A = 1$). The temperature field drives a single-cell circulation centred at $x = 0.56, z = 0.32$ with inflow to the cavity through the upper surface for $x < 0.51$ and outflow for $x > 0.51$. The vertical heat flux Q calculated from the leading contribution to (2.9) as $R \to 0$ is given from (3.5) as

$$Q = \frac{1}{3A} + O(R), \quad R \to 0. \tag{3.10}$$

The equivalent results for a cosine profile

$$S(x) = \tfrac{1}{2}(1 - \cos(\pi x)) \tag{3.11}$$

are given by Adamou-Graham (2008).

https://doi.org/10.1017/jfm.2012.34 Published online by Cambridge University Press

4. Numerical solution for general Darcy–Rayleigh numbers

The steady-state system (2.2), (2.3) and (2.6)–(2.8) is elliptic but a simple method of finding solutions is to introduce artificial time derivatives to obtain the system

$$\frac{\partial \psi}{\partial t} = \nabla^2 \psi + R\frac{\partial T}{\partial x}, \quad \frac{\partial T}{\partial t} = \nabla^2 T - \frac{\partial (T, \psi)}{\partial (x, z)}, \tag{4.1}$$

which is parabolic in time. This allows a numerical solution to be found by a straightforward marching procedure, with the required steady-state results obtained in the limit of large time. An explicit forward difference method was used to solve (4.1) and (2.6)–(2.8) together with an initial condition usually taken as $\psi = 0, T = S(x)(1 - (z/A))$ at $t = 0$. The equations were discretized on a uniform grid using standard second-order accurate central difference approximations for the spatial derivatives and forward differences for the time derivatives. In discretizing the boundary conditions for $\partial T/\partial x$ and $\partial \psi/\partial z$ second-order accuracy was maintained by using a quadratic interpolation to evaluate T or ψ on the boundaries. The time step was chosen small enough to ensure numerical stability. Various checks were carried out with different spatial grid sizes to test the accuracy and temporal convergence of the scheme, and most of the results described here were obtained with step sizes of 0.0025 in x and z and a time step of 10^{-6}. For $R = 1000$, convergence of the solution to its steady-state form occurred to 6 significant figures in the values of ψ and T when $t = 0.4$. The heat flux integral (2.9) was calculated using Simpson's rule and its value monitored at $z = 0, A/2$ and A as a further check on accuracy.

For base temperature profiles with $S'(1) \neq 0$ there is a weak logarithmic singularity in the vertical temperature gradient at the lower boundary as $x \to 1-$. This is because the value of $\partial T/\partial x(x, 0)$ must adjust from the value $S'(1)$ to zero on the vertical wall $x = 1$. The adjustment is achieved via a local solution of Laplace's equation in which

$$T = 1 + f_0(\zeta) r \ln r + f_1(\zeta) r + \cdots, \quad r \to 0, \tag{4.2}$$

where r, ζ are polar coordinates with $1 - x = r\cos\zeta, z = r\sin\zeta$ and

$$f_0 = a_0 \sin\zeta, \quad f_1 = a_1 \sin\zeta + b_1 \cos\zeta + a_0 \zeta \cos\zeta, \tag{4.3}$$

where a_0, a_1 and b_1 are constants. A consistent solution for f_1 satisfying $f_1(0) = -S'(1)$ and $f_1'(\pi/2) = 0$ requires that $b_1 = -a_0\pi/2 = -S'(1)$ and it follows that

$$\frac{\partial T}{\partial z}(x, 0) \sim \frac{2}{\pi} S'(1) \ln(1 - x), \quad x \to 1-. \tag{4.4}$$

Note that the heat flux integral (2.9) remains convergent at $x = 1$. Because $\partial T/\partial z$ is evaluated only at internal grid points in the finite difference scheme and because the singularity is weak, it was not found to require any special treatment in the numerical scheme.

Contours of the steady-state stream function and temperature fields for a square cavity ($A = 1$) with the quadratic temperature profile (2.10) are shown in figure 2 for $R = 100$ and 2000. At smaller values of R the results were found to be consistent with the analytical results of § 3, with the contours indistinguishable from those of figure 1 in the case when $R = 1$. For large R the flow is seen to develop a boundary layer structure in which the temperature variation is confined to a horizontal boundary layer along the lower surface and a plume adjacent to the hot sidewall. Figure 3 shows the total vertical heat flux Q as a function of R for a square cavity. Other properties of the numerical solutions are compared with an asymptotic solution for large R in the next section.

https://doi.org/10.1017/jfm.2012.34 Published online by Cambridge University Press

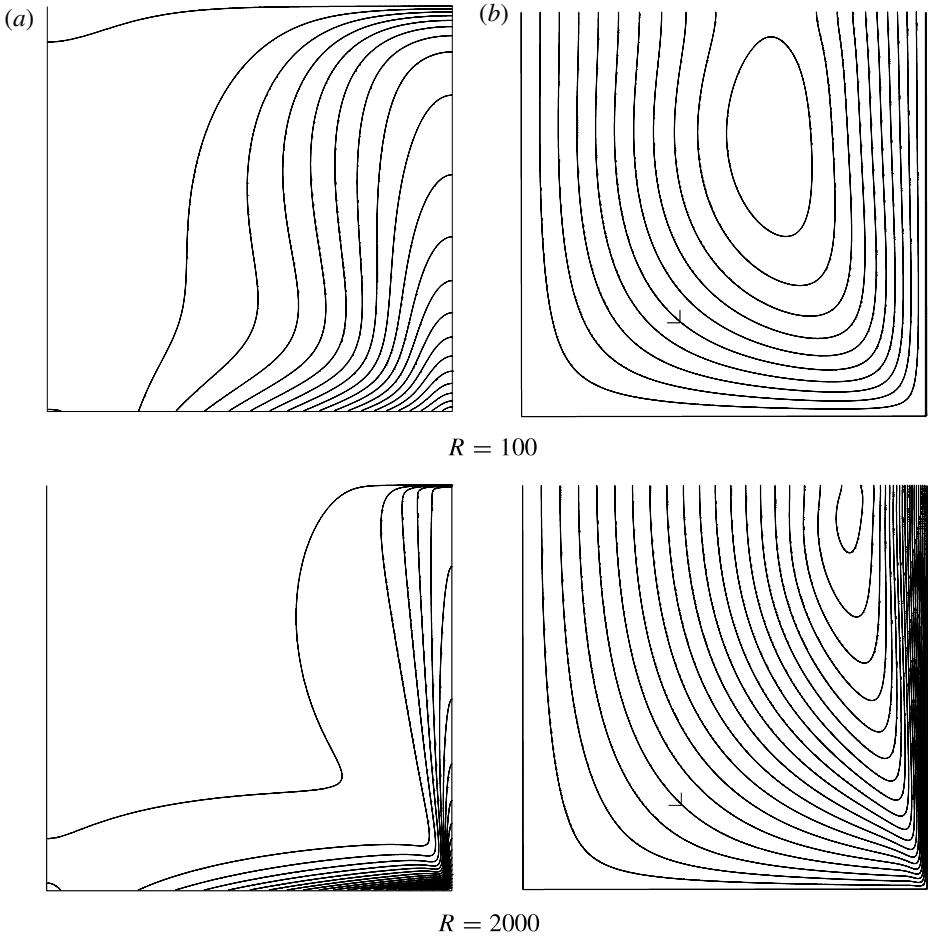


FIGURE 2. Contours of T (a) and ψ (b) for a square cavity ($A = 1$) with the quadratic profile (2.10) and $R = 100$ and 2000. Temperature contours are shown for $T = 0.001$ and at intervals of 0.05 from $T = 0.05$ to 1.

5. Solution for large Darcy–Rayleigh numbers

A schematic diagram of the proposed asymptotic structure of the solution in the limit of large Darcy–Rayleigh number is shown in figure 4. The numerical results indicate that the flow assumes a boundary layer structure in which heat enters the base and is conveyed to the hot end of the cavity by a horizontal boundary layer (region I in figure 4). Here it ascends, initially in the corner zone II and then in a narrow plume (region III) before leaving through the upper surface via the upper surface layer IV. Fluid entering the cavity through the upper surface is drawn across the main core region (region V) and is entrained by the plume where it rises and leaves through the upper surface.

5.1. *Horizontal boundary layer*

Near the lower surface there is a horizontal boundary layer in which

$$T = \theta(x, Z) + \cdots, \quad \psi = R^{1/3}\phi(x, Z) + \cdots, \quad R \to \infty, \tag{5.1}$$

https://doi.org/10.1017/jfm.2012.34 Published online by Cambridge University Press

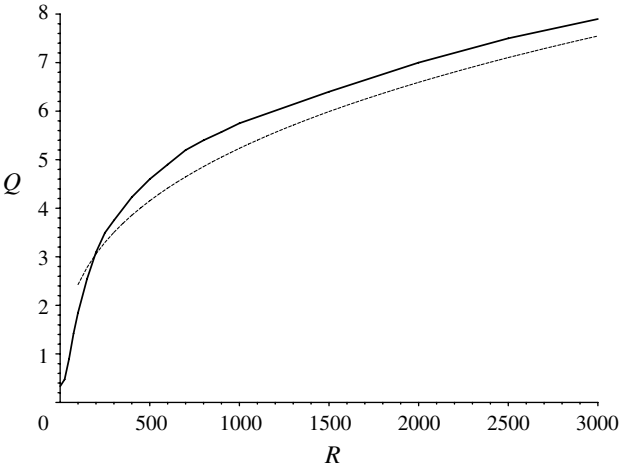


FIGURE 3. Total heat flux Q as a function of R for a square cavity ($A = 1$) with the quadratic temperature profile (2.10). Also shown (by the dashed curve) is a large R asymptotic prediction obtained in (5.8) below.

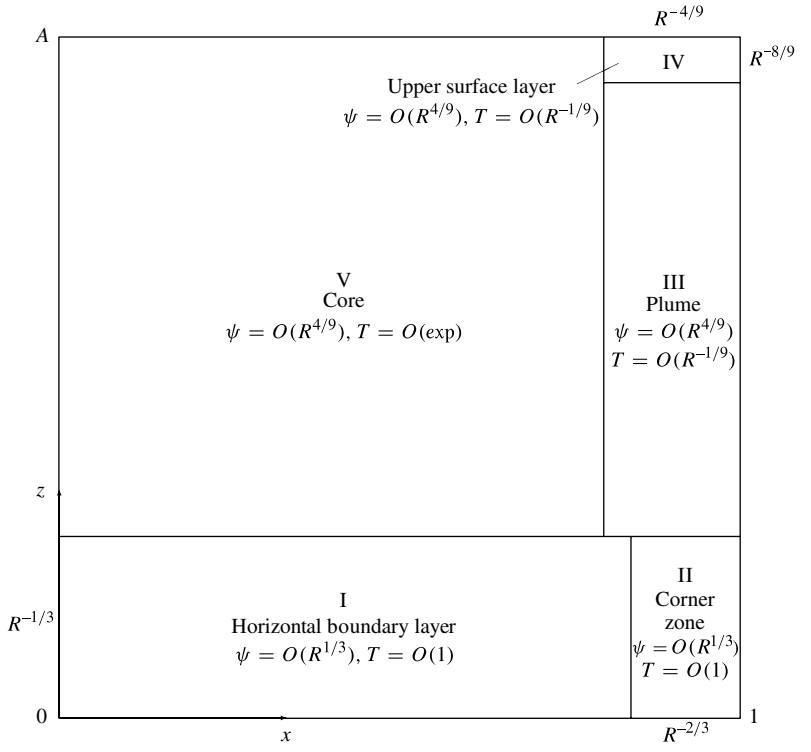


FIGURE 4. Schematic diagram of the main regions of the asymptotic structure of the solution as $R \to \infty$.

where $z = R^{-1/3}Z$. Here the scalings of ψ and z with R are needed to ensure a balance between vertical conduction and convection in the heat equation and between

https://doi.org/10.1017/jfm.2012.34 Published online by Cambridge University Press

horizontal shear and buoyancy in the vorticity equation. Thus, the functions θ and ϕ satisfy the equations

$$\frac{\partial^2\phi}{\partial Z^2} = -\frac{\partial\theta}{\partial x}, \quad \frac{\partial^2\theta}{\partial Z^2} = \frac{\partial(\theta,\phi)}{\partial(x,Z)}, \tag{5.2}$$

with boundary conditions

$$\theta = S(x), \quad \phi = 0 \quad \text{on } Z = 0, \tag{5.3}$$

$$\phi = 0, \quad \frac{\partial\theta}{\partial x} = 0 \quad \text{on } x = 0, \tag{5.4}$$

$$\theta \to 0, \quad \frac{\partial\phi}{\partial Z} \to 0 \quad \text{as } Z \to \infty. \tag{5.5}$$

Here (5.3) are the lower wall conditions, (5.4) assumes that both wall conditions at the cold sidewall can be applied directly to the horizontal boundary layer solution, consistent with the first equation in (5.2), and (5.5) assumes that both the temperature and horizontal velocity must tend to zero at the upper edge of the layer. This is because the core region, to be considered in § 5.5, is isothermal and contains a circulation generated by entrainment into the plume, for which the stream function is weaker than order $R^{2/3}$. Further discussion of this is given in a summary of the overall asymptotic structure in § 6.

For the quadratic profile (2.10), the system (5.2)–(5.5) has a similarity solution

$$\phi = x\phi_0(Z), \quad \theta = x^2\theta_0(Z), \tag{5.6}$$

where $\phi_0'' = -2\theta_0$, $\theta_0'' = 2\phi_0'\theta_0 - \phi_0\theta_0'$. Elimination of θ_0 and one integration in Z shows that ϕ_0 satisfies the system

$$\phi_0''' + \phi_0\phi_0'' - \tfrac{3}{2}\phi_0'^2 = 0, \quad \phi_0(0) = 0, \quad \phi_0''(0) = -2, \quad \phi_0'(\infty) = 0. \tag{5.7}$$

The solution found by Daniels & Punpocha (2004) has the properties $\phi_0'(0) = c = 1.447$ and $\phi_0 \sim a - k\mathrm{e}^{-aZ}$, $\theta_0 \sim b\mathrm{e}^{-aZ}$ as $Z \to \infty$ where $a = 1.141$, $k = 1.021$, $b = ka^2/2 = 0.665$. Graphs of ϕ_0, ϕ_0' and $\theta_0 = -\phi_0''/2$ are shown in figure 5. Since $\theta_0'(0) = -\phi_0'''(0)/2 = -3\phi_0'(0)^2/4 = -3c^2/4$, the heat flux (2.9) through the base can be calculated as

$$Q \sim R^{1/3}Q_0, \quad R \to \infty, \tag{5.8}$$

where

$$Q_0 = -\int_0^1 \frac{\partial\theta}{\partial Z}(x,0)\,\mathrm{d}x = -\theta_0'(0)\int_0^1 x^2\,\mathrm{d}x = \frac{1}{4}c^2. \tag{5.9}$$

At the hot end of the horizontal boundary layer, $x = 1$, this has been converted into a horizontal convective heat flux

$$\int_0^\infty \left(\theta\frac{\partial\phi}{\partial Z}\right)_{x=1}\mathrm{d}Z = \int_0^\infty \theta_0\phi_0'\,\mathrm{d}Z = Q_0 \tag{5.10}$$

that now enters the corner zone II. The asymptotic result (5.8), (5.9) is shown in figure 3 and is consistent with the numerical calculations of § 4.

Figure 6 shows the local heat transfer and slip velocity at the lower boundary given by (5.6), along with the numerical results of § 4 for various values of R. It is seen that the numerical results approach the asymptotic limit as R increases. The intricate behaviour of the numerical results for the local heat transfer as $x \to 1$ is associated

https://doi.org/10.1017/jfm.2012.34 Published online by Cambridge University Press

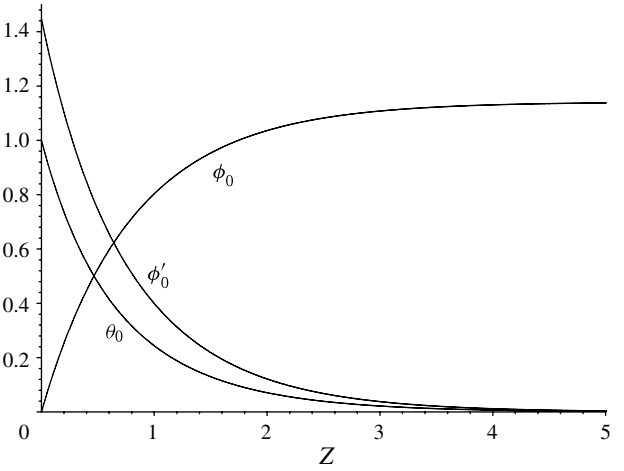


FIGURE 5. The functions ϕ_0, ϕ_0' and θ_0 of the horizontal boundary layer solution.

with the logarithmic singularity in $\partial T/\partial z(x, 0)$ discussed in § 4. This behaviour of the full governing system is not observed in the horizontal boundary layer solution because that solution does not extend into the corner of the cavity.

5.2. *Corner zone*

Here the solution is given by

$$T = \Theta(X, Z) + \cdots, \quad \psi = R^{1/3}\Phi(X, Z) + \cdots, \quad R \to \infty, \tag{5.11}$$

where $x = 1 - R^{-2/3}X$. The scalings of ψ and z are dictated by those entering this region from the horizontal boundary layer, while that of x ensures a balance between horizontal conduction and convection in the heat equation, and vertical shear and buoyancy in the vorticity equation. Thus, the functions Θ and Φ satisfy the vertical boundary layer equations

$$\frac{\partial^2\Phi}{\partial X^2} = \frac{\partial\Theta}{\partial X}, \quad \frac{\partial^2\Theta}{\partial X^2} = \frac{\partial(\Theta, \Phi)}{\partial(Z, X)}, \tag{5.12}$$

with boundary conditions

$$\Phi = 0, \quad \frac{\partial\Theta}{\partial X} = 0 \quad \text{on } X = 0, \tag{5.13}$$

$$\Phi \to \Phi_\infty = \phi_0(Z), \quad \Theta \to \Theta_\infty = \theta_0(Z) \quad \text{as } X \to \infty, \tag{5.14}$$

$$\Phi = 0, \quad \Theta = 1 \quad \text{on } Z = 0. \tag{5.15}$$

Here (5.13) are the sidewall boundary conditions, the edge conditions (5.14) are specified by matching with the solution in the horizontal boundary layer at $x = 1$, and (5.15) are specified by the conditions at the lower boundary.

Integration of the heat equation in (5.12) across the layer and use of (5.13)–(5.15), together with integration in Z upwards from the lower boundary, shows that at a general depth Z,

$$\int_0^\infty \Theta \frac{\partial\Phi}{\partial X}\,\mathrm{d}X = \int_0^Z \theta_0\phi_0'\,\mathrm{d}Z. \tag{5.16}$$

https://doi.org/10.1017/jfm.2012.34 Published online by Cambridge University Press

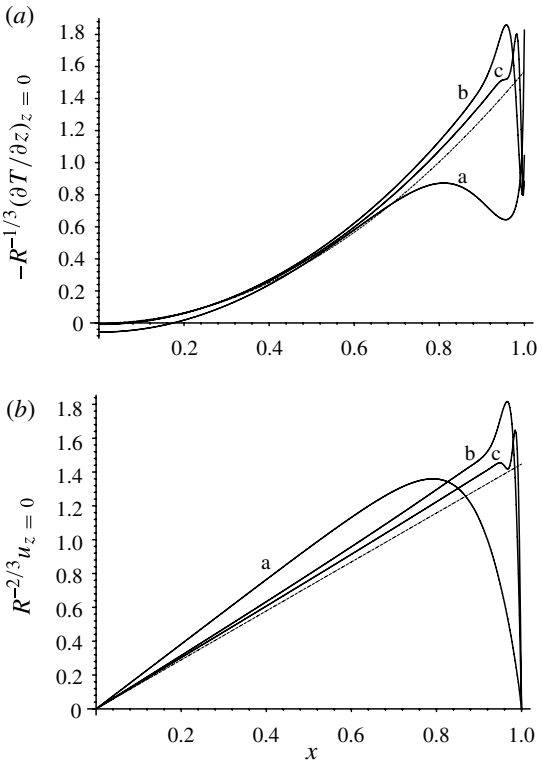


FIGURE 6. Scaled local heat transfer (*a*) and slip velocity (*b*) at the lower boundary given by the numerical results for a square cavity ($A = 1$) with the quadratic temperature profile (2.10) and (a) $R = 100$, (b) $R = 1000$, (c) $R = 3000$. The dashed curves are the large R asymptotic predictions given by the horizontal boundary layer solution (5.6).

This expresses the fact that the upward vertical heat flux in the layer must equal the horizontal flux entering from the horizontal boundary layer. At the top of the corner region all of the heat transported from the base of the cavity by the horizontal boundary layer has entered the corner zone, so that making use of (5.10),

$$\int_0^\infty \Theta \frac{\partial \Phi}{\partial X}\,\mathrm{d}X \to \int_0^\infty \theta_0 \phi_0'\,\mathrm{d}Z = Q_0 \quad \text{as } Z \to \infty. \tag{5.17}$$

Another feature of the corner problem (5.12)–(5.15) is the question of whether the horizontal boundary layer profiles at the edge of the layer admit solutions with exponential decay to the forms (5.14) as $X \to \infty$ that enable the two wall conditions (5.13) to be satisfied. From (5.12) this exponential behaviour is associated with the real part of the form $\mathrm{e}^{-\lambda(Z)X}$ where

$$\lambda = \lambda_\pm = \tfrac{1}{2}(\phi_0' \pm (\phi_0'^2 + 4\theta_0')^{1/2}). \tag{5.18}$$

Since $\phi_0' > 0$ and $\theta_0' < 0$ for all $0 \leqslant Z < \infty$ the two roots λ_+ and λ_- both have positive real parts indicating that a solution satisfying the two wall conditions (5.13) is possible. The profiles ϕ_0 and θ_0 in figure 5 are such that $\phi_0'^2 + 4\theta_0' < 0$ for all Z so that in general there is an oscillatory decay to the outer profiles in (5.14). At small Z, $\lambda_\pm \sim c(1 \pm \sqrt{2}\mathrm{i})/2$ and at large Z, $\lambda_\pm \sim (ak\mathrm{e}^{-aZ} \pm \sqrt{2}\mathrm{i}k^{1/2}a^{3/2}\mathrm{e}^{-aZ/2})/2$, with the latter

https://doi.org/10.1017/jfm.2012.34 Published online by Cambridge University Press

indicating an exponential widening of the layer as $Z \to \infty$. This, together with the flow reversal at the edge of the layer, makes a numerical solution of the full system (5.12)–(5.15) difficult, but further insight can be gained by considering the asymptotic structure of the solution as $Z \to \infty$. Details of this are given in an Appendix and indicate that a double structure develops. Near the wall, where $\eta = X/Z^{2/3}$ is finite, the Wooding (1963) similarity solution

$$\Phi \sim Z^{1/3} f(\eta), \quad \Theta \sim Z^{-1/3} g(\eta), \quad Z \to \infty, \tag{5.19}$$

emerges, where

$$f = q \tanh\left(\frac{q\eta}{6}\right), \quad g = \frac{1}{6} q^2 \operatorname{sech}^2\left(\frac{q\eta}{6}\right), \tag{5.20}$$

and $q = (9Q_0)^{1/3}$ is determined by the heat flux requirement (5.17). Further from the wall there is an exponentially wide outer region containing a weak downflow that feeds the upward motion associated with (5.19), (5.20). Because the temperature field is exponentially small in this outer region, there is no significant contribution to the heat flux.

5.3. *Plume*

Here the solution is given by

$$T = R^{-1/9} \tilde{T}(\tilde{X}, z) + \cdots, \quad \psi = R^{4/9} \tilde{\psi}(\tilde{X}, z) + \cdots, \quad R \to \infty, \tag{5.21}$$

where $x = 1 - R^{-4/9}\tilde{X}$ and the scalings in R are determined by expressing the plume solution (5.19) in terms of the vertical cavity scale z. The functions $\tilde{T}$ and $\tilde{\psi}$ satisfy the vertical boundary layer equations and to a first approximation the solution that matches with the corner region II is simply a continuation of the plume solution (5.19), (5.20). Thus

$$\tilde{T} = \frac{1}{6} z^{-1/3} q^2 \operatorname{sech}^2\left(\frac{q\tilde{X}}{6z^{2/3}}\right), \quad \tilde{\psi} = z^{1/3} q \tanh\left(\frac{q\tilde{X}}{6z^{2/3}}\right). \tag{5.22}$$

The temperature decays exponentially into the core region V and the mass flux is supplied by entrainment from the core, requiring that $\psi \sim qR^{4/9} z^{1/3}$ as $R \to \infty$ in the core region at $x = 1$. The core solution is considered in § 5.5.

Figure 7 shows the wall temperature and slip velocity given by (5.21) and (5.22), along with the numerical results of § 4 for various values of R. The numerical results approach the asymptotic limit as R increases, with departures due to the presence of the corner region near $z = 0$ and in the temperature field near the upper surface. The plume structure has been observed in experimental studies of the flow above a heated line source reported by Cheng (1985) and Masuoka *et al.* (1986).

5.4. *Upper surface layer*

When the plume reaches the upper surface of the cavity, an adjustment is needed to accommodate the boundary conditions $T = \partial\psi/\partial z = 0$ on $z = A$. The main adjustment occurs on a shallow scale of order $R^{-8/9}$ close to the surface where the solution has the form

$$T = R^{-1/9} \tilde{\Theta}(\tilde{X}, \tilde{Z}) + \cdots, \quad \psi = R^{4/9} \tilde{\Phi}(\tilde{X}, \tilde{Z}) + \cdots, \quad R \to \infty \tag{5.23}$$

and $z = A - R^{-8/9}\tilde{Z}$. Here the scalings of T, ψ and x are determined by those of the plume solution at $z = A$, while that of z is dictated by the need for vertical conduction

https://doi.org/10.1017/jfm.2012.34 Published online by Cambridge University Press

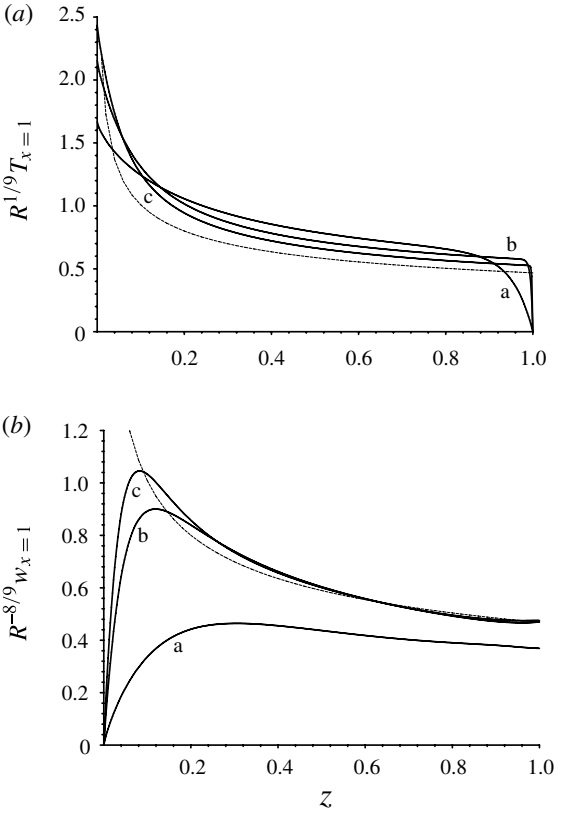


FIGURE 7. Scaled wall temperature (a) and slip velocity (b) at $x = 1$ given by the numerical results for a square cavity ($A = 1$) with the quadratic temperature profile (2.10) and (a) $R = 100$, (b) $R = 1000$, (c) $R = 3000$. The dashed curves are the large R asymptotic predictions given by the plume solution (5.22).

to balance convection. Because the resulting vertical scale is small compared with the plume width, vertical shear, horizontal conduction and buoyancy can all be neglected to a first approximation. Thus, the governing equations for $\tilde{\Phi}$ and $\tilde{\Theta}$ are

$$\frac{\partial^2\tilde{\Phi}}{\partial\tilde{Z}^2} = 0, \quad \frac{\partial^2\tilde{\Theta}}{\partial\tilde{Z}^2} = \frac{\partial(\tilde{\Theta},\tilde{\Phi})}{\partial(\tilde{X},\tilde{Z})} \tag{5.24}$$

and the solution for $\tilde{\Phi}$ that matches with the plume solution (5.21) as $\tilde{Z} \to \infty$ and satisfies the upper surface condition $\partial\tilde{\Phi}/\partial\tilde{Z} = 0$ at $\tilde{Z} = 0$ is simply

$$\tilde{\Phi} = A^{1/3} q \tanh\left(\frac{q\tilde{X}}{6A^{2/3}}\right), \tag{5.25}$$

representing the upward flow generated by the plume. The temperature field $\tilde{\Theta}$ now satisfies

$$\frac{\partial^2\tilde{\Theta}}{\partial\tilde{Z}^2} = -\frac{\mathrm{d}\tilde{\Phi}}{\mathrm{d}\tilde{X}}\frac{\partial\tilde{\Theta}}{\partial\tilde{Z}}, \tag{5.26}$$

https://doi.org/10.1017/jfm.2012.34 Published online by Cambridge University Press

and so the solution that matches with the plume solution as $\tilde{Z} \to \infty$ and satisfies the surface condition $\tilde{\Theta} = 0$ is

$$\tilde{\Theta} = \frac{q^2}{6A^{1/3}} \operatorname{sech}^2\left(\frac{q\tilde{X}}{6A^{2/3}}\right)\left(1 - \exp\left\{-\frac{q^2\tilde{Z}}{6A^{1/3}} \operatorname{sech}^2\left(\frac{q\tilde{X}}{6A^{2/3}}\right)\right\}\right). \tag{5.27}$$

The isotherms rising through the plume are turned abruptly to intersect the sidewall at depths of order $R^{-8/9}$ from the upper surface. Heat transfer out of the upper surface is achieved through the conductive contribution $Q \sim R^{1/3} \int_0^\infty \partial\tilde{\Theta}/\partial\tilde{Z}(\tilde{X}, 0)\, \mathrm{d}\tilde{X}$ in (2.9) which is equal to $Q_0 R^{1/3}$ from (5.27) and completes the vertical transfer of heat through the cavity.

The leading contribution to the horizontal velocity u in the upper surface layer is generated by buoyancy and vertical shear in the vorticity equation. Thus, $u = \partial\psi/\partial z \sim R^{4/9}\tilde{U}(\tilde{X}, \tilde{Z})$ where

$$\frac{\partial\tilde{U}}{\partial\tilde{Z}} = \frac{\partial^2\tilde{\Phi}}{\partial\tilde{X}^2} - \frac{\partial\tilde{\Theta}}{\partial\tilde{X}}. \tag{5.28}$$

The solution found subject to the requirement that $\tilde{U} = 0$ at $\tilde{Z} = 0$ is

$$\tilde{U} = -\frac{q^3\tilde{Z}}{18A} \operatorname{sech}^2\left(\frac{q\tilde{X}}{6A^{2/3}}\right) \tanh\left(\frac{q\tilde{X}}{6A^{2/3}}\right) \exp\left\{-\frac{q^2\tilde{Z}}{6A^{1/3}} \operatorname{sech}^2\left(\frac{q\tilde{X}}{6A^{2/3}}\right)\right\}. \tag{5.29}$$

Note that this approaches zero as $\tilde{Z} \to \infty$ and is negative over the depth of the layer, so that it has the effect of displacing the plume streamlines away from the sidewall slightly as they rise through the layer. This is because the fluid is cooled as it approaches the upper surface and is thus slowed by buoyancy, leading to a local widening of the plume.

A further adjustment to the order $R^{4/9}$ contribution to u occurs on a larger vertical scale near the upper surface. This is because (5.29) vanishes at the lower edge of the upper surface layer, whereas the horizontal velocity $u \sim R^{4/9}\partial\tilde{\psi}/\partial z$ associated with the plume solution (5.21), (5.22) is non-zero as $z \to A-$. This adjustment occurs in an upper corner region whose depth is comparable with the width of the plume. Because the solution there has no impact on the leading order solutions for ψ and T in the cavity, the details are not considered here.

5.5. *Core region*

Here the temperature field is exponentially small and the flow field is generated by entrainment into the plume. From (5.21), this determines the stream function as

$$\psi = R^{4/9}\Psi(x, z) + \cdots, \quad R \to \infty, \tag{5.30}$$

where Ψ satisfies Laplace's equation

$$\frac{\partial^2\Psi}{\partial x^2} + \frac{\partial^2\Psi}{\partial z^2} = 0 \tag{5.31}$$

and the boundary conditions

$$\Psi = 0 \quad \text{on } z = 0, \qquad \frac{\partial\Psi}{\partial z} = 0 \quad \text{on } z = A, \tag{5.32}$$

$$\Psi = 0 \quad \text{on } x = 0, \qquad \Psi = qz^{1/3} \quad \text{on } x = 1. \tag{5.33}$$

https://doi.org/10.1017/jfm.2012.34 Published online by Cambridge University Press

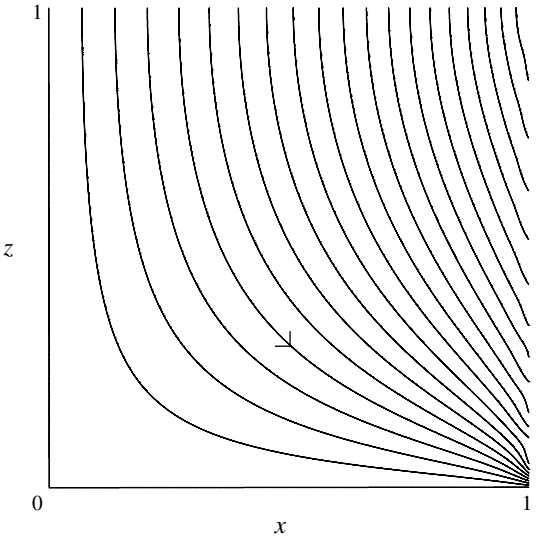


FIGURE 8. Core streamlines for a square cavity ($A = 1$).

The required solution is

$$\Psi = A^{1/3} q \sum_{m=0}^{\infty} b_{2m+1} \frac{\sinh \dfrac{(2m+1)\pi x}{2A} \sin \dfrac{(2m+1)\pi z}{2A}}{\sinh \dfrac{(2m+1)\pi}{2A}}, \tag{5.34}$$

where

$$b_{2m+1} = 2 \int_0^1 \bar{z}^{1/3} \sin \frac{(2m+1)\pi \bar{z}}{2} \, \mathrm{d}\bar{z}. \tag{5.35}$$

Figure 8 shows the core streamlines for a square cavity ($A = 1$); the stream function at the upper surface of the core ($z = A$) and the slip velocity at the sidewall $x = 0$ are shown in figure 9, along with the corresponding numerical results for various values of R obtained in § 4. The presence of the plume is evident near $x = 1$ and in the limit as $R \to \infty$ the vortex centre of the flow moves to the hot end of the upper surface, located at the junction of the core and the edge of the plume.

It is interesting to observe that the boundary conditions (5.32), (5.33) imply a discontinuity in $\partial\Psi/\partial z$ at the upper corner $x = 1, z = A$, leading to a weak logarithmic singularity there in the solution of Laplace's equation for Ψ. In fact, this singularity is similar to that described by (4.2)–(4.4) for the temperature field in the lower hot corner of the cavity, but with the roles of x and z reversed. The core slip velocity $\partial\Psi/\partial x$ at $x = 1$ has a logarithmic singularity as $z \to A$ that influences the corrections to ψ and T in the plume of order one and $R^{-5/9}$ respectively, and hence also the structure of the upper corner region mentioned at the end of § 5.4.

6. Summary

Numerical and asymptotic solutions for cavity flow in a porous medium driven by monotonic differential heating of the lower surface have been found for a range of Darcy–Rayleigh numbers. For an upper surface held at constant pressure and constant

https://doi.org/10.1017/jfm.2012.34 Published online by Cambridge University Press

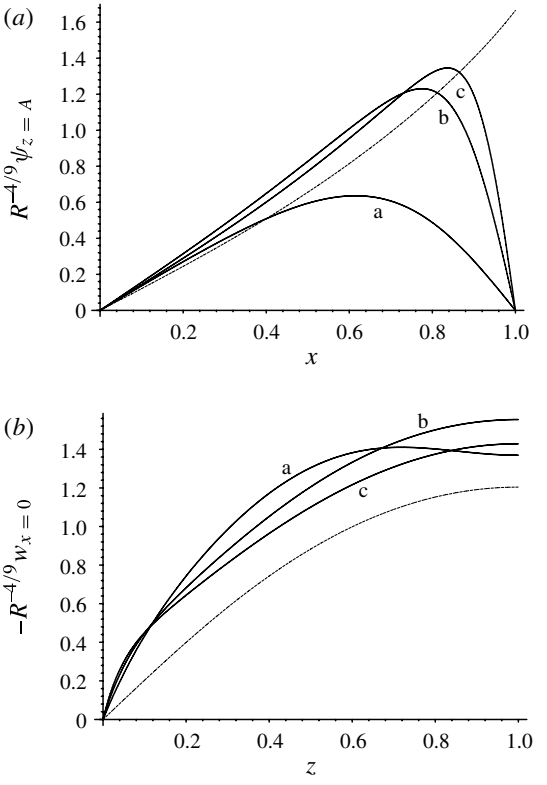


FIGURE 9. Scaled stream function (*a*) on $z = A$ and slip velocity (*b*) on $x = 0$ for a square cavity ($A = 1$) with the quadratic temperature profile (2.10) and (a) $R = 100$, (b) $R = 1000$, (c) $R = 3000$. The dashed curves are the large R asymptotic predictions given by the core solution (5.34).

temperature equal to the minimum temperature of the lower surface, a single-cell circulation is generated, the centre of which moves to the upper corner of the cavity on the hot side as the Darcy–Rayleigh number increases. The main features of the limiting structure of the solution as $R \to \infty$ have been determined and, as shown in figure 3, predict an overall heat transfer consistent with the numerical calculations for the quadratic temperature profile (2.10).

Other features of the large R limiting structure also compare well with the numerical results, as shown in figures 6, 7 and 9. In figure 6, the slip velocity and the local heat transfer at the lower boundary show convergence towards the linear and quadratic forms predicted by the horizontal boundary layer solution of § 5.1, except near the hot corner where locally the corner zone solution of region II takes over. Here the horizontal flow is brought rapidly to rest as the plume develops at the vertical wall. The wall temperature and slip velocity predicted by the plume solution are consistent with the trend of the numerical results, as shown in figure 7, and there is a local departure from the asymptotic solution of § 5.3 both near $z = 0$ where the corner zone solution applies and near $z = A$ where the wall temperature adjusts within the upper surface layer. This latter adjustment occurs very close to the upper surface, as predicted by the asymptotic solution of § 5.4, whereas the development of the plume in the lower corner occurs over a much longer vertical scale. This has quite a significant

https://doi.org/10.1017/jfm.2012.34 Published online by Cambridge University Press

impact on the core solution, reducing the actual entrainment relative to that predicted by the plume solution. As shown in figure 9, this in turn reduces both the mass flux entering the top of the cavity and the vertical slip velocity at the cold wall in comparison with the asymptotic solution in the core given in § 5.5. At the lower edge of the core, the discrepancy in figure 9 between the vertical slip velocity at the wall $x = 0$ and the asymptotic core solution also reflects a relatively large correction there (of relative order $R^{-1/9}$ as $R \to \infty$) caused by the presence of the horizontal boundary layer.

The large R structure shown in figure 4 is not a complete asymptotic description. The analysis of § 5 and the Appendix suggests that the corner zone II contains an exponentially widening region as $Z \to \infty$ in which the temperature is exponentially small. In practice this expansion of the layer must be limited by the breakdown of the vertical boundary layer equations governing region II and this occurs when the width of the layer becomes comparable with its depth. Since the expansion of the layer is exponential, this occurs at depths of order $R^{-1/3} \ln R$, only slightly greater than the depth of the main horizontal layer, allowing a local adjustment of the solution to match with the core solution in the lower hot corner.

Another feature of the large R asymptotic structure not explored in detail here is the matching of the solution at the lower edge of the core region as $z \to 0$ and in the horizontal boundary layer as $Z \to \infty$. In the horizontal boundary layer it is required that the gradient $\partial\phi/\partial Z$ of the leading order stream function tends to zero as $Z \to \infty$; otherwise, the core would contain a stream function of order $R^{2/3}$ which, being larger than that generated by entrainment into the plume, would have homogeneous boundary conditions on all boundaries, leading to a null solution of Laplace's equation. The horizontal boundary layer then generates an order $R^{1/3}$ contribution to ψ as $Z \to \infty$ which produces a correction of this magnitude to the order $R^{4/9}$ core stream function generated by the plume. In order to match with the horizontal boundary layer, the leading order core stream function Ψ must vanish at $z = 0$, as stipulated in (5.32). Since Ψ is linear in z as $z \to 0$, it in turn generates a correction term in ψ of order $R^{1/9}$ in the horizontal boundary layer. Thus, the proposed structure leads to a consistent solution in which the core and horizontal boundary layer contain corrections of relative order $R^{-1/9}$ and $R^{-2/9}$, respectively.

The range of Darcy–Rayleigh numbers considered in the present study is consistent with that encountered in geothermal systems. For water percolating through various types of rock, typical values of the permeability K range from 10^{-11} cm^2 in granite to 10^{-8} cm^2 in sandstone and limestone (Brace 1980) with values as high as 10^{-6} cm^2 or more if significant fracturing is present (Phillips 1991, Ch. 2) as in the fissured rocks of a caldera (Chery *et al.* 1991). Typical values of the other physical parameters relevant in geothermal flows can be taken as

$$\left.\begin{aligned} &\gamma = 2 \times 10^{-4}/^{\circ}\mathrm{C}, \quad \kappa = 1.4 \times 10^{-3}\ \mathrm{cm}^2\ \mathrm{s}^{-1}, \quad \nu = 10^{-2}\ \mathrm{cm}^2\ \mathrm{s}^{-1}, \\ &d = 1\ \mathrm{km}, \quad \Delta T = 100\,^{\circ}\mathrm{C}, \end{aligned}\right\} \tag{6.1}$$

giving values of the Darcy–Rayleigh number R defined by (2.4) ranging from 1.4 to 1400 as the permeability K ranges from 10^{-11} to 10^{-8} cm^2.

In terms of limitations to the present results, the two main effects that may impinge on the validity of Darcy's law are inertial (Forchheimer) effects and no-slip (Brinkman) effects (see, for example, Nield & Bejan 1999, Ch. 1). The former can be

https://doi.org/10.1017/jfm.2012.34 Published online by Cambridge University Press

ignored if the Reynolds number based on pore width is small,

$$Re = \frac{UK^{1/2}}{\nu} \ll 1, \tag{6.2}$$

where U is the maximum speed of the flow, and the latter can be ignored if

$$K^{1/2} \ll L, \tag{6.3}$$

where L is the smallest length scale of the flow. In the present case, U and L are both associated with the flow in the corner zone II. The maximum flow speed occurs at the vertical wall and can be estimated from the results of figure 7. In non-dimensional form, this gives $w \sim 0.429R$, at $z \sim R^{-1/3}z_0$, where $z_0 = 1.20$, and thus

$$U \sim 0.429R\kappa/d, \quad R \to \infty. \tag{6.4}$$

At the same location, the minimum width of the corner zone can be estimated by dividing the mass flux by the vertical speed. Using the results of figure 5, this gives the non-dimensional width as $1-x \sim R^{1/3}\phi_0(z_0)/w \sim (0.871R^{1/3})/(0.429R) = 2.03R^{-2/3}$, so that

$$L \sim 2.03R^{-2/3}d, \quad R \to \infty. \tag{6.5}$$

Substitution of (6.4) and (6.5) into (6.2) and (6.3) and use of the parameter values listed in (6.1) indicates that inertial effects can be ignored if

$$RK^{1/2} \ll 1.67 \times 10^6 \text{ (cm)} \tag{6.6}$$

and that no-slip effects can be ignored if

$$R^{2/3}K^{1/2} \ll 2.03 \times 10^5 \text{ (cm)}. \tag{6.7}$$

These are comfortably satisfied for the range of Darcy–Rayleigh numbers R and permeabilities K relevant to the geothermal flows considered here.

Of more significance is the effect of non-constant fluid properties that can be expected for the large range of temperatures encountered in typical geothermal flows. Effects of variable viscosity and thermal expansion were considered originally in the context of heating from below by Morland, Zebib & Kassoy (1977) and Straus & Schubert (1977) and have been studied more recently, for example, by Nield (1996).

Although the results described here focus on the case of a quadratic temperature profile (2.10) at the lower surface, numerical calculations for other monotonic profiles such as the cosine profile (3.11) (Adamou-Graham 2008) indicate that a similar boundary layer structure emerges as the Darcy–Rayleigh number increases. Thus, the precise form of the temperature profile is not expected to be significant and in a geothermal setting would be determined by the nature of the underlying magma chamber. The profile (3.11) has a local maximum at $x = 1$ and so produces a less intense flow around the lower hot corner than the quadratic profile (2.10). For these weaker flow rates the solution becomes susceptible to a wavelike instability so that at $R = 3000$, for example, the solution for a square cavity with the cosine profile (3.11) exhibits a time-dependent oscillation at the end of the horizontal boundary layer that propagates into the plume, as shown in figure 10. Further work is needed to investigate more precisely the conditions under which such instability occurs, although it is possible to gain some insight by considering the behaviour at the edge of the corner region where the steady-state solution is characterized by the exponential decay $e^{-\lambda(Z)X}$ as $X \to \infty$ with λ given by (5.18). The Darcy equations governing time-dependent

https://doi.org/10.1017/jfm.2012.34 Published online by Cambridge University Press

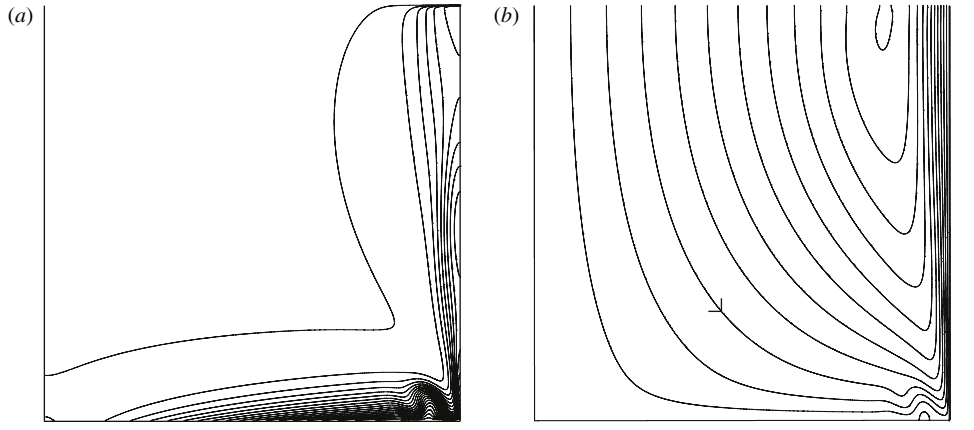


FIGURE 10. Contours of an unsteady solution of (4.1) at $t = 1.5$ for T (a) and ψ (b) for a square cavity ($A = 1$) with the cosine profile (3.11) at $R = 3000$. Temperature contours are shown for $T = 0.001$ and at intervals of 0.05 from $T = 0.05$ to $T = 1$.

flow are given by (4.1) with the term $\partial\psi/\partial t$ omitted and if the non-dimensional time t is scaled by writing $t = R^{-4/3}\tau$, the second equation in (5.12) then contains an additional term $\partial\Theta/\partial\tau$ on the right-hand side. The stability of the solution at the edge of the corner region can then be investigated by considering time-dependent solutions of the form $\mathrm{e}^{-\lambda(Z)X+\omega\tau}$ as $X \to \infty$, leading to an equation for the growth rate ω given by

$$\omega = \lambda^2 - \lambda\phi_0' - \theta_0'. \tag{6.8}$$

The steady-state solutions $\lambda_\pm$ given by (5.18) correspond to $\omega = 0$ and nearby solutions can be considered by setting $\lambda = \lambda_\pm + \bar{\lambda}$ with $\bar{\lambda}$ small. Linearization of (6.8) then gives

$$\omega = \pm\bar{\lambda}\,(\phi_0'^2 + 4\theta_0')^{1/2}. \tag{6.9}$$

Since $\phi_0'^2 + 4\theta_0' < 0$ this indicates that a general disturbance for which $\bar{\lambda}$ contains an imaginary part, corresponding to a small change of wavelength in X, leads to a component of the solution that grows in time. This suggests that the corner flow is unstable in the limit as $R \to \infty$ and hence that it will lose stability as R increases, consistent with the behaviour found numerically.

It is also likely that three-dimensional effects become significant as the Darcy–Rayleigh number increases. Much work has been done on the sequence of transitions from steady to unsteady flow in the context of the Darcy–Bénard problem (see, for example, Rees 2000) and the transition to time-dependent and three-dimensional vortex states has been studied in the context of free convective boundary layers and plume flows in a variety of geometries (see, for example, Rees 2002). An investigation of the stability of the corner flow involved in the present work is a particularly difficult prospect because the basic steady-state solution is not known analytically. Further progress will therefore require a considerable numerical effort to compute the basic solution and to investigate its stability.

https://doi.org/10.1017/jfm.2012.34 Published online by Cambridge University Press

Appendix. An approximate solution in the corner region as $Z \to \infty$

Given the heat flux constraint (5.17) together with the governing equations (5.12), the main balance as $Z \to \infty$ requires that Θ, Φ and X are of order $Z^{-1/3}$, $Z^{1/3}$ and $Z^{2/3}$, respectively, suggesting a solution of the form

$$\Phi \sim Z^{1/3} f(\eta), \quad \Theta \sim Z^{-1/3} g(\eta), \quad Z \to \infty, \tag{A 1}$$

where $\eta = X/Z^{2/3}$. This cannot encompass the entire behaviour of the solution as $Z \to \infty$ because it does not incorporate the exponential growth of the layer or the explicit forms of ϕ_0 and θ_0 as $Z \to \infty$. However, because it is a solution of the full equations consistent with the heat flux condition, it can be used to provide a useful *approximation* to the asymptotic structure of the solution for large Z. If it is assumed that

$$\Phi_\infty \sim \alpha Z^{1/3}, \quad \Theta_\infty \sim \beta Z^{-1/3}, \quad Z \to \infty, \tag{A 2}$$

then the required behaviour is equivalent to replacing the constants α and β by $\alpha = aZ^{-1/3} \ll 1$ and $\beta = bZ^{1/3}\mathrm{e}^{-aZ} \ll 1$. From (5.12), (5.14) and (A 1), f and g satisfy the equations

$$f' = g - \beta, \quad g'' = -\tfrac{1}{3}(f'g + fg'). \tag{A 3}$$

One integration of the second equation and use of the wall conditions $f = g' = 0$ at $\eta = 0$ gives $g' = -fg/3$ and then removal of the parameter β through the transformations

$$f(\eta) = \beta^{1/2} F(\xi), \quad g(\eta) = \beta G(\xi), \quad \eta = \beta^{-1/2}\xi, \tag{A 4}$$

gives

$$P\frac{\mathrm{d}P}{\mathrm{d}F} = -\frac{1}{3}F(P+1), \tag{A 5}$$

where $P = G - 1 = F'$. One further integration gives

$$F^2 - \delta^2 = 6(\ln|1+P| - P), \tag{A 6}$$

where δ is a constant of integration such that $F^2 = \delta^2$ at $P = 0$. For a given value of δ, (A 6) defines a curve in the (P, F^2) plane starting from $F^2 = 0$ at $P = P_1 > 0$, increasing to $F^2 = \delta^2$ at $P = 0$ and then decreasing to $F^2 = 0$ at $P = P_2$, where $-1 < P_2 < 0$. Since it is required that

$$Q_0 = \int_0^\infty gf'\,\mathrm{d}\eta = \beta^{3/2}\int_0^\infty GP\,\mathrm{d}\xi \tag{A 7}$$

is finite, and β is small, the relevant solution of (A 6) is one for which δ is large, in which case the logarithmic term on the right-hand side can be neglected to a first approximation in the region $P > 0$. This gives

$$F \sim \delta\tanh\left(\frac{\delta\xi}{6}\right), \quad G \sim P \sim \frac{1}{6}\delta^2\mathrm{sech}^2\left(\frac{\delta\xi}{6}\right) \tag{A 8}$$

as $\delta \to \infty$. Evaluation of the integral in (A 7) then gives

$$Q_0 = \tfrac{1}{9}\beta^{3/2}\delta^3, \tag{A 9}$$

https://doi.org/10.1017/jfm.2012.34 Published online by Cambridge University Press

so that the relevant limit is $\beta \to 0, \delta \to \infty$ such that $\beta^{1/2}\delta$ remains finite and in the original variables (A 4),

$$f = q \tanh\left(\frac{q\eta}{6}\right), \quad g = \frac{1}{6}q^2 \mathrm{sech}^2\left(\frac{q\eta}{6}\right), \tag{A 10}$$

where $q = (9Q_0)^{1/3}$. This is the similarity solution for a vertical plume with finite heat flux Q_0 originally found by Wooding (1963). The stream function rises from zero at the wall to the value q as $\eta \to \infty$, representing an upward flow adjacent to the wall with the vertical velocity and temperature field reaching exponentially small values as $\eta \to \infty$. Because α is required to be small in (A 2), this upward mass flux must be counterbalanced by a downward flow further from the wall. This corresponds to an alternative balance as $\delta \to \infty$ in which the logarithmic term dominates on the right-hand side of (A 6). This occurs if $P \approx -1$ and corresponds to the region $P < 0$ in (A 6). Assuming that $F \to \delta$ as $\xi \to 0$, this gives $F \sim \delta - \xi$ for $0 < \xi < \delta$ and then from (A 6), $G = 1 + P \sim \exp(-\delta^2 D(\xi/\delta))$ where

$$D\left(\frac{\xi}{\delta}\right) \sim \frac{1}{6}\left(\frac{\xi}{\delta}\right)\left(2 - \frac{\xi}{\delta}\right) + o(1) \quad \text{as } \delta \to \infty. \tag{A 11}$$

Thus, in the original variables,

$$f \sim q\left(1 - \frac{\beta\eta}{q}\right), \quad g \sim \beta \exp\left\{-\beta^{-1}q^2 D\left(\frac{\beta\eta}{q}\right)\right\}, \quad 0 < \eta < \beta^{-1}q. \tag{A 12}$$

This represents a linearly decreasing stream function on the exponentially large scale η of order β^{-1} over which the temperature field remains exponentially small. This region provides the downflow needed to supply the upward motion adjacent to the wall. Because the temperature field is exponentially small, there is no significant contribution to the heat flux integral (A 7) from this region.

The above analysis indicates a possible asymptotic structure as $Z \to \infty$ consistent with the development of the Wooding (1963) plume on an inner scale X of order $Z^{2/3}$ adjacent to the sidewall with the mass flux supplied mainly by a slow downflow over an outer exponentially wider scale in X, augmenting that supplied by the horizontal boundary layer. Although the analysis assumes α and β to be constant and so cannot be a formally correct description of the asymptotic structure in the outer region, it suggests that the corner region can accommodate the necessary transition of the flow and temperature fields from the horizontal boundary layer into the vertical plume on the sidewall.

REFERENCES

ADAMOU-GRAHAM, P. 2008 Plume flows in porous media driven by horizontal differential heating, PhD thesis, City University London.

BRACE, W. F. 1980 Permeability of crystalline and argillaceous rocks. *Int. J. Rock Mech. Min. Sci.* **17**, 241–251.

CHENG, P. 1985 Natural convection in a porous medium: external flows. In *Natural Convection: Fundamentals and Applications* (ed. S. Kakac, W. Aung & R. Viskanta). Hemisphere.

CHERY, J., BONNEVILLE, A., VILOTTE, J. P. & YUEN, D. 1991 Numerical modelling of caldera dynamic behaviour. *Geophys. J. Intl* **105**, 365–379.

DANIELS, P. G. 2007 On the boundary layer structure of differentially heated cavity flow in a stably stratified porous medium. *J. Fluid Mech.* **586**, 347–370.

DANIELS, P. G. & PUNPOCHA, M. 2004 Cavity flow in a porous medium driven by differential heating. *Intl J. Heat Mass Transfer* **47**, 3017–3030.

https://doi.org/10.1017/jfm.2012.34 Published online by Cambridge University Press

DANIELS, P. G. & PUNPOCHA, M. 2005 On the boundary-layer structure of cavity flow in a porous medium driven by differential heating. *J. Fluid Mech.* **532**, 321–344.

DANIELS, P. G. & SIMPKINS, P. G. 1984 The flow induced by a heated vertical wall in a porous medium. *Q. J. Mech. Appl. Maths* **37**, 339–354.

HORTON, C. W. & ROGERS, F. T. 1945 Convection currents in a porous medium. *J. Appl. Phys.* **16**, 367–370.

INGHAM, D. B. & BROWN, S. N. 1986 Flow past a suddenly heated vertical plate in a porous medium. *Proc. R. Soc. Lond.* **A403**, 51–80.

INGHAM, D. B., MERKIN, J. H. & POP, I. 1982 Flow past a suddenly cooled vertical flat surface in a saturated porous medium. *Intl J. Heat Mass Transfer* **25**, 1916–1919.

INGHAM, D. B. & POP, I. 1987 Free convection from a semi-infinite vertical surface bounded by a horizontal wall in a porous medium. *Intl J. Heat Mass Transfer* **30**, 1615–1622.

JOSHI, V. & GEBHART, B. 1984 Vertical natural convection flows in porous media: calculations of improved accuracy. *Intl J. Heat Mass Transfer* **27**, 69–75.

KOHOUT, F. A. 1965 A hypothesis concerning cyclic flow of salt water related to geothermal heating in the Floridian aquifer. *Trans. N. Y. Acad. Sci.* **28**, 249–271.

MASUOKA, T., TOHDA, Y., TSUROTA, Y. & YASUDA, Y. 1986 Buoyant plume above concentrated heat source in stratified porous media. *Trans. JSME Ser.* B **52**, 2656–2662.

MERKIN, J. H. 1980 Mixed convection boundary layer flow on a vertical surface in a saturated porous medium. *J. Engng Maths* **14**, 301–313.

MORLAND, L. W., ZEBIB, A. & KASSOY, D. R. 1977 Variable property effects on the onset of convection in an elastic porous material. *Phys. Fluids* **20**, 1255–1259.

NIELD, D. A. 1996 The effect of temperature-dependent viscosity on the onset of convection in a saturated porous medium. *Trans. ASME: J. Heat Transfer* **118**, 803–805.

NIELD, D. A. & BEJAN, A. 1999 *Convection in Porous Media*. Springer.

PHILLIPS, O. M. 1991 *Flow and Reactions in Permeable Rocks*. Cambridge University Press.

REES, D. A. S. 2000 The stability of Darcy–Bénard convection. In *Handbook of Porous Media* (ed. K. Vafai). Marcel Dekker.

REES, D. A. S. 2002 Recent advances in the instability of free convective boundary layers in porous media. In *Transport Phenomena in Porous Media II* (ed. D. B. Ingham & I. Pop). Elsevier.

REES, D. A. S. & BASSOM, A. P. 1991 Some exact solutions for free convection flows over heated semi-infinite surfaces in porous media. *Intl J. Heat Mass Transfer* **34**, 1564–1567.

REES, D. A. S. & BASSOM, A. P. 1993 The nonlinear non-parallel wave instability of boundary-layer flow induced by a horizontal heated surface in porous media. *J. Fluid Mech.* **253**, 267–296.

REES, D. A. S. & BASSOM, A. P. 1994 The linear wave instability of boundary-layer flow induced by a horizontal heated surface in porous media. *Intl Commun. Heat Mass Transfer* **21**, 143–150.

STRAUS, J. M. & SCHUBERT, G. 1977 Thermal convection of water in a porous medium: effects of temperature- and pressure-dependent thermodynamic and transport processes. *J. Geophys. Res.* **82**, 325–333.

WOODING, R. A. 1963 Convection in a saturated porous medium at large Rayleigh number or Péclet number. *J. Fluid Mech.* **15**, 527–544.

https://doi.org/10.1017/jfm.2012.34 Published online by Cambridge University Press